LOW-COST BIO-INNOVATIVE TITANIUM ALLOYS FOR DENTAL IMPLANT APPROACHES (A COMPARATIVE IN VITRO – IN VIVO ANIMAL STUDY)

Dawlat Mostafa *[iD], Yasser Abdelrhman**[iD], Sengo Kobayashi ***[iD], Samia Soliman Omar****[iD] *and* Mohamed Gepreel*****[iD]

ABSTRACT

Background: Titanium is widely used for dental implants due to its superior mechanical properties, low density, and biocompatibility. While Ti-6Al-4V (Grade V) is a standard implant alloy, concerns over aluminum and vanadium toxicity have led to the development of alternative alloys. This study evaluates the biocompatibility and osseointegration of two cost-effective, vanadium-free titanium alloys: β-type Ti–4.7Mo–4.5Fe (TMF55) and (α+β)-type Ti–3Mo–0.5Fe (TMF31), compared to Grade V titanium.

Materials and methods: Three titanium alloys—Grade V (control), TMF55, and TMF31—were fabricated. Discs (8mm × 3mm) and implant cylinders (3mm × 6mm) were used for in vitro (EDX, XRD, Young's modulus, cytotoxicity, cell viability) and in vivo (histology, histomorphometry, osteopontin expression) assessments. BIC% was analyzed after 2 and 6 weeks in V Spain white rabbits.

Results: EDX and XRD confirmed alloy composition. TMF31 demonstrated a significantly lower Young's modulus (P<0.0001), higher cell viability at 6 hours (P=0.0001) and 7 days (P=0.04), strong osteopontin expression, and comparable BIC% to Grade V (P>0.1). In contrast, TMF55 showed lower Young's modulus (P<0.0001), reduced cell viability (P<0.0001), weak osteopontin expression, and lower BIC% at 2 and 6 weeks (P=0.001).

Conclusions: TMF31 emerges as a promising, cost-effective alternative to Grade V titanium for dental implants, whereas TMF55 is unsuitable due to poor osseointegration and biocompatibility.

KEYWORDS: Dental implants, titanium alloys, osseointegration, biocompatibility, vanadium-free.

* Assistant Professor of Dental Biomaterials, College of Dentistry, The Arab Academy for Science and Technology and Maritime Transport, El-Alamein. (AASTMT/ El-Alamein), Egypt.

** Department of Design and Production Engineering, Assiut University, Assiut, 71515, Egypt. Mechanical and Industrial Engineering Department, College of Engineering, Majmaah University, Al Majmaah, 11952, Saudi Arabia

*** Professor of Materials Science and Biotechnology, Egypt-Japan University of Science and Technology, Alexandria, Egypt.

**** Oral Biology Department, Faculty of Dentistry, Alexandria University, Alexandria, Egypt.

**** Material Science and Engineering Department, Egypt, Japan University of Science and Technology, Alexandria, Egypt.

INTRODUCTION

Implant dentistry has seen significant scientific progress over the last five decades, despite its short history, rapid research and technological advancements have propelled it to become a cornerstone of contemporary dentistry. Over the past 50 years, both surgical and restorative approaches to implants have evolved considerably, giving rise to new challenges and requirements for improved therapeutic results, as well as enhanced educational and training opportunities. The substantial economic influence of implant dentistry has spurred extensive industrial growth, resulting in the continuous release of new implant systems, restorative options, and technological innovations on an annual basis [1].

A dental implant serves as a device embedded within the jawbone to facilitate the transmission of bite force. The crucial biological requirement for implant success is achieving osseointegration. Researchers have devoted significant effort over the years to experimenting with various implant materials to ensure both biocompatibility and favorable biological properties. In the initial phases of clinical investigation, Brånemark pioneered the use of titanium screw-type implants with a machined surface, proposing the osseointegration theory, a pivotal contribution that sparked substantial advancements in oral implantology. However, the Schroeder International Team employed implants featuring a titanium plasma-sprayed surface. Since then, an increasing array of implant materials has been introduced for clinical applications [2].

Appropriately, the process of osseointegration encompasses a cascade of biological events. Following the placement of implant into bone, inflammatory and immune responses are triggered, afterwards angiogenesis and osteogenesis follow. It is understood that the initial stage towards osseointegration is achieving primary stability, typically attained during implant placement. Secondary stability is established as a result of healing and new bone formation. Throughout this sequence, the physical and chemical characteristics of the implant, such as its topography and hydrophilicity, play a critical role in facilitating the binding of blood proteins, which create cell attachment sites via integrin receptors. Consequently, neutrophils adhere to implant surface, with monocytes and macrophages then arriving within 2 to 4 days [3].

Over two thirds of implants utilized consist of metallic biomaterials, including stainless steel, cobalt (Co)-chromium (Cr) alloys, and titanium (Ti) and its alloys Since the 1960s, both commercially pure (Cp) and alloyed versions of titanium have been recognized as the preeminent biomaterials for endosseous dental implants, earning them the designation of the "gold standard" owing to their low density, lightweight, remarkable corrosion resistance, impressive strength-to-weight ratio, favorable tribological properties, and exceptional biocompatibility [4].

Most endosseous dental implants and zygomatic implants are constructed from unalloyed commercially pure titanium (cpTi) of various grades. There are four types of cpTi utilized in the production of dental implants (Grade I, Grade II, Grade III, and Grade IV) with titanium purity ranging from 98% to 99.6%, distinguished by their varying oxygen content and properties such as corrosion resistance, ductility, and strength. Grade I cpTi boasts the highest purity and formability, while grade IV offers the highest strength coupled with moderate formability [5]. A material ideal for dental implant fabrication should exhibit biocompatibility and possess sufficient strength, toughness, as well as fracture and corrosion resistance. These characteristics are often linked to oxygen presence in the metal. Grade IV CpTi, with 0.4% oxygen, offers exceptional strength, making it the most utilized titanium type for dental implants [6]. Another alloy commonly used in the field of implantology is Ti-6Al-4V, occasionally referred to as grade V

titanium. It is favored for its remarkable strength as well as its satisfactory biological acceptance [7].

The titanium oxide (TiO2) layer covering implant surface is a crucial factor contributing to its exceptional biocompatibility. This nanometric layer confers resistance to corrosion and renders titanium bioinert in vivo, thereby facilitating acceptable osseointegration [8]. However, literature discussions highlight potential issues associated with titanium implant characteristics within the patient's body, such as hypersensitivity or peri-implant bone overload. Titanium boasts an elastic modulus (E-modulus) of 110 GPa, while cortical bone registers an elastic modulus of 13.8 GPa and spongy bone 1.38 GPa. This variance concerns potential mechanical overload on the bone, leading to damage to the surrounding parent bone and subsequent bone resorption known as "stress-shielding". Additionally, corrosion represents another challenge commonly associated with titanium and titanium alloy implants, as no metal or alloy is entirely resistant to corrosion [9].

Titanium alloys incorporate various alloying elements, primarily categorized into alpha (α) stabilizers like carbon, nitrogen, oxygen, and aluminum, and beta (β) stabilizers such as iron, vanadium, cobalt, and nickel. Consequently, dental titanium alloys are available in three structural forms: α, β, or a combination of both (α+β). The α+β combination alloy, notably Ti-6Al-4V, is the most prevalent in dental applications. Comprising 6% aluminum and 4% vanadium, Ti-6Al-4V exhibits high strength and corrosion resistance [10,11]. On the other hand, this alloy releases aluminum and vanadium, both of which have the potential to induce biological issues as aluminum disrupts bone mineralization, which can result in structural deficiencies, while vanadium exhibits cytotoxicity and has the potential to induce type IV allergic reactions [6].

Consequently, the trend in titanium alloy fabrication is shifting towards β-titanium alloys

following studies suggesting potential toxicity of Ti-6Al-4V. Additionally, in certain alloys like Ti-13.4Al-29Nb, the breakdown of the passive layer is linked to elevated aluminum content that is poorly absorbed in the gastrointestinal tract, with only a minimal amount entering the bloodstream. Therefore, there is a growing desire for low-cost titanium alloys characterized by high biocompatibility and low elastic modulus [5].

Based on the previously mentioned, there has been a growing inclination towards the development of vanadium-free titanium alloys with reduced rigidity, boasting high biocompatibility, exceptional corrosion resistance, elevated strength, and an elastic modulus comparable to that of human bone. The lower Young's modulus of β-Ti alloys, which may mitigate the "stress-shielding" effect, has spurred researchers to explore a variety of β-type Ti-alloys, such as Ti–13Nb–13Zr, Ti–12Mo–6Zr–2Fe (TMZF), Ti–15Mo, Ti–Nb17Ta6O1 (TNTO) and Ti–29Nb–13Ta–4.6Zr (TNTZ) for potential biomedical applications. However, many of these alloys contain costly elements like Ta, Nb, and Zr. Subsequently, researchers have redirected towards developing cost-effective titanium alloys for biomedical approaches, either utilizing universal elements or reducing the inclusion of costly rare elements. Examples include Ti–3Zr–5Fe–5Mo, Ti–Cr, and Ti–Mn alloys [12].

By leveraging Bo–Md electronic parameters, researchers have engineered a V-free beta titanium alloy that offers compelling advantages over the traditional Ti–6Al–4V alloy. These alloys were strategically designed to be situated near the phase boundary in the $\overline{Bo}$ - $\overline{Md}$ diagram. One alloy, with a composition of Ti-3Mo-0.5Fe atomic percent (designated as TMF31), is positioned in the upper region proximate to the martensitic transformation boundary within the $\overline{Bo}$ - $\overline{Md}$ diagram. The other alloy, with a composition of Ti-4.74Mo-4.5Fe atomic percent (designated as TMF55), is located at

the periphery of the single β phase field. Compared to the Ti–6Al–4V dental implant alloy, these developed vanadium-free titanium alloys significantly reduce raw material costs by approximately 50%, underscoring their economic feasibility without compromising performance. Consequently, TMF55 and TMF31 emerge as promising alternatives to Ti–6Al–4V for specific biomedical applications. Their combination of mechanical strength, cost-efficiency, and tailored properties positions them as compelling candidates for various implant applications, offering both functional and economic advantages [13]. This advancement highlights the critical role of biomaterial innovation in the evolution of healthcare technologies.

From this standpoint, the present research aims to conduct a comparative analysis involving laboratory testing, cytotoxicity evaluations, and experimental histological assessments of the low cost-effective and bio-innovative (β)-type Ti–4.7Mo–4.5Fe (TMF55) alloy and (α+β)-type Ti – 3Mo – 0.5Fe (TMF31) in conjunction with the conventional Ti–6Al–4V (Grade V) alloy. The objective is to assess their biocompatibility and osseointegration bioactivity, particularly concerning their potential for dental implant applications. The null hypothesis for this study posited that there are no significant differences in the biocompatibility, cytotoxicity, and osseointegration bioactivity among the TMF55 alloy, TMF31 alloy, and the conventional Ti–6Al–4V (Grade V) alloy for dental implant applications.

MATERIALS AND METHODS

Sample size calculations

Sample size was calculated based on a previous study and by using Med Calc statistical software. Assuming t-test to be 1.96, an alpha of 0.05 and power of study 90.0%. A typical advice is to reject the null hypothesis H0 if the corresponding p-value is smaller than 0.05. The study required a minimum sample size of 36 implant cylinders for each healing period, with 6 implants allocated to each subgroup. Furthermore, each laboratory test necessitated a minimum sample size of 18 discs, with 6 discs assigned to each group.

Design and preparation of titanium alloys specimens (discs and implant cylinders)

Three titanium dental implant alloys were prepared; (α+β)-type Ti–6Al–4V (Grade V) titanium implant alloy that used as the control, and two designed alloys, the (β)-type Ti–4.7Mo–4.5Fe (TMF55) and the (α+β)-type Ti–3Mo–0.5Fe (TMF31). Alloys production was conducted by melting high purity sing an electric-arc furnace with a tungsten electrode on a water-cooled copper hearth under argon atmosphere (ARCAST200, USA). The ingots (~ 100 g) of the alloys were melted and inverted six times to promote their homogeneity. They were next hot-rolled at 800-850 ℃ into 5 mm-thick plates, leading to a total deformation reduction of approximately 60%. Then, specimens were cut in to discs (8mmx3mm) (N=90) and implant cylinders (3mmx6mm) (N=90) using EDM wire cutting (Makino UX3, USA). All samples were solid solution-treated (ST) at 900 ℃/1hr under inert gas condition for 1.2 ks, followed by rapid quenching in ice water. Subsequently, all prepared specimens of the three titanium alloys were surface polished up to 2000 mesh, then subjected to ultrasonic cleaning (T-14, L&R manufacturer, USA) with distilled water and acetone for 15 minutes to remove any potential contaminants before further testing.

Grouping

The titanium discs prepared totaled 90, alongside 72 implant cylinders were randomly divided into three equal groups. One group served as the control, consisting of the Ti–6Al–4V alloy, and another two test groups featured low-cost, bio-innovative alloys named TMF55 and TMF31, (n = 30 discs – n = 24 implants cylinders for each group). Regarding vitro characterizations, six discs were used per group

for each test, (n=6). It is emphasized that each implant group was divided into two subgroups, each containing 12 implants. One subgroup was allocated for histological assessment, while the other subgroup was designated for histomorphometric analysis. These histological and histomorphometric assessments were conducted twice for two healing periods, within each implant subgroup, six implant cylinders were tested after a 2-week period, and the other six were tested after a 6-week healing period, (n= 6). For the immunohistochemical assessment of the three titanium alloys studied after a 2-week healing period, a total of 18 implant cylinders were utilized, with 6 implants assigned to each alloy group (n=6). So, a total of 90 implant cylinders were used.

In vitro Characterization

The elemental composition of both control and test titanium specimens was examined using energy-dispersive X-ray (EDX) analysis (INCA Penta FETX3, Model 6583, OXFORD Instruments, England). The analysis was performed on uncoated samples at 20 kV. Phase identification of the studied alloys was conducted by Cu-Kα X-ray diffractometry using a diffractometer (XRD-6100, Shimadzu, Japan) operating at 30 kV and 30 mA in a 2θ range of 30-80 degrees. Mechanical characterization was performed to investigate Young's moduli. A free resonance device (FQ 2000 - MORI Engineering. Co., Ltd., Japan) was used to measure the Young's modulus at room temperature in air [14].

Cytotoxicity-Biocompatibility laboratory test

The cytotoxicity test was conducted in triplicates according to ISO 10993-5:2009. The murine-derived MC3T3-E1 cell line (provided by Riken BioResource Center Co., Ltd., Japan) was adopted to evaluate the cytotoxicity of the control and test titanium groups via direct cell assays (CCK-8 assay). Ti discs were autoclaved at 120 $^{\circ}$C for 30 min under dry conditions. MC3T3-E1 cells were

cultured in Eagle's minimal essential medium (MEM-α) (Wako Pure Chemical Co., Ltd., Japan) supplemented with 10% fetal bovine serum (FBS) and 1% penicillin-streptomycin and incubated in a humidified atmosphere with 5% CO_2 at 37 $^{\circ}$C. The culture medium was replenished every 3 days. After the short culture period (i.e., 6 h), the cell size and shape indexes were examined. Cell viability, measured by the number of attached MC3T3-E1 cells, was analyzed for the control and test implant alloys using ImageJ software (version 2.14.0, NIH, USA) following incubation periods of 6 hours and 7 days.

In vivo experimental animal phase

Thirty-six male line V Spain white rabbits, aged six months and weighing 3 kg, were acquired in a good health from the Poultry Research Center at the Faculty of Agriculture, Alexandria University. Rabbits were randomly assigned into three groups (N= 12) equivalent to the implant groups including control group (Ti–6Al–4V), TMF55 and TMF31 test groups. Similarly, another nine rabbits were employed for immunohistochemical evaluation of the studied groups following a 2-week healing period. All implant cylinders were sterilized with gamma radiation (25 KG) prior to surgical placement. Two implant cylinders were surgically placed in the femurs of each rabbit, with one being inserted into the distal head of the right femur and the other into the corresponding region of the left femur.

All surgical interventions were conducted under general anesthesia and in strictly aseptic environments. Rabbits were anesthetized using intramuscular injections of ketamine and xylazine at doses of 35 mg/kg and 5 mg/kg of body weight, respectively. A surgical flap was carefully reflected to expose the distal head of the femur, followed by sequential drilling of implant sockets with adequate cooling at room temperature to minimize trauma. Each implant was then inserted, and the surgical flap

was repositioned and sutured. Following the surgical procedure, rabbits administered intramuscular injections of a broad-spectrum antibiotic and analgesic every 72 hours for a period of 10 days. Daily monitoring was conducted to assess weight gain and observe cage behavior. The implants were permitted to undergo a healing process lasting for 2 and 6 weeks prior to the rabbits being sacrificed [15].

Prior to euthanasia, midazolam (5 mg/kg, IV) was used for sedation, followed by IV administration of pentobarbital ≥120 mg/kg for euthanasia. After the animals were euthanized either at 2 or 6 weeks, decalcified histological sections were produced for histological assessment. This involved fixing the femoral heads, containing the implants, in 10% neutral buffered formalin for one week, followed by complete decalcification of the bone in 8% trichloroacetic acid. Subsequently, the decalcified bone segments underwent standard processing procedures [16].

Two longitudinal cuts opposite each other around each implant were made for the extraction of the osseointegrated implants. Subsequently, each bone segment was halved to facilitate implant removal. These halves were then encased in molten wax to obtain 5-μm longitudinal sections of the bone edge parallel to the implant space. Following this, the sections were stained using hematoxylin and eosin stain (H&E) for histological analysis under a light microscope. Furthermore, immunohistochemical evaluation was conducted to investigate peri-implant osteopontin expression at the two-week period of implant healing [17]. On the other hand, histomorphometric analysis was performed by preparation of undecalcified bone histological sections. The implant containing bone blocks were processed through a series of procedures, starting with fixation and dehydration, followed by embedding in transparent methyl methacrylate monomer. Then, sectioned using a precision cutting machine equipped with a diamond-coated

disc (Micracut 150, Metkon metallography, Turkey) resulting in 150-μm-thick sections. These sections were then polished using silicon carbide and stained with Stevenel's Blue and van Gieson picrofuchsin. Histomorphometric analysis and calculation of bone-to-implant contact percentage (BIC%) were accomplished on the mid-section of each implant using digital images obtained from a stereo stereomicroscope (Olympus imaging digital camera, model E.330 DC 7. 4 V, Japan). The images were analyzed using computer software program (Olympus. Cell ^A). The percentage of mature bone stained red in contact with the implant diameter was measured as a proportion of the entire implant diameter to determine the bone implant contact percentage of control and test groups [18].

Statistical analysis

Data was fed to the computer using IBM SPSS software package version 24.0. The Shapiro–Wilk test was used to test of normality of data, the data of BIC% was parametric data, the Kolmogorov-Smirnov and Shapiro–Wilk had p value >0.05. For normally distributed data, comparison between two independent population were done using independent t-test while more than two population were analyzed F-test (ANOVA) to be used, followed by post hoc test (Mann Whitney test) to compare between each two groups. Significant test results are quoted as two-tailed probabilities. The significance of the results obtained was judged at the 5% level.

RESULTS

Laboratory tests results

The results of the energy-dispersive X-ray (EDX) analysis for the three studied groups are presented in Table [1] and Figure [1]. The mean atomic percentage of vanadium (V) for the control group was 12.13 with a standard deviation (SD) 0.29. For the TMF55 and TMF31 test groups, vanadium (V) was not detected; instead, iron (Fe)

and molybdenum (Mo) were observed. The mean atomic percentage of Fe was 2.51 with an SD 0.07 for TMF55, and 0.36 with SD 0.01 for TMF31. The mean atomic percentage of Mo was 2.83 with SD 0.03 for TMF55, and 1.70 with SD 0.01 for TMF31. There was a statistically significant increase in the mean atomic percentages of Fe and Mo from the TMF31 to TMF55 alloys (P <0.0001).

TABLE (1) Comparison of atomic percentages of iron and molybdenum in TMF55 and TMF31 implant alloys as determined by EDX analysis

	TMF55 Implant Alloy (n=6)	TMF31 Implant Alloy (n=6)
Iron (Fe)		
Range	2.39-2.55	0.35-0.37
Mean	2.51	0.36
S.D.	0.07	0.01
P value	<0.0001*	
Molybdenum (Mo)		
Range	2.79-2.86	1.68-1.72
Mean	2.83	1.70
S.D.	0.03	0.01
P value	<0.0001*	

P was significant if ≤0.05

*Significant difference at level 0.05

The XRD patterns of control group (Ti–6Al–4V), TMF55 and TMF31 titanium implant alloys following solution treatment at 900°C (ST900) are shown in Figure [2]. The XRD pattern of the control titanium alloy after ST900 treatment shows the detection of both α (alpha) and β (beta) phases. For the TMF55 alloy, the β (beta) phase is clearly the predominant phase, accompanied by a minor amount of α (alpha) orthorhombic martensite phase. In contrast, after the ST900 treatment of the TMF31 alloy, the predominant phase formed was mainly the α (alpha) orthorhombic martensite phase with insignificant β-phase [19].
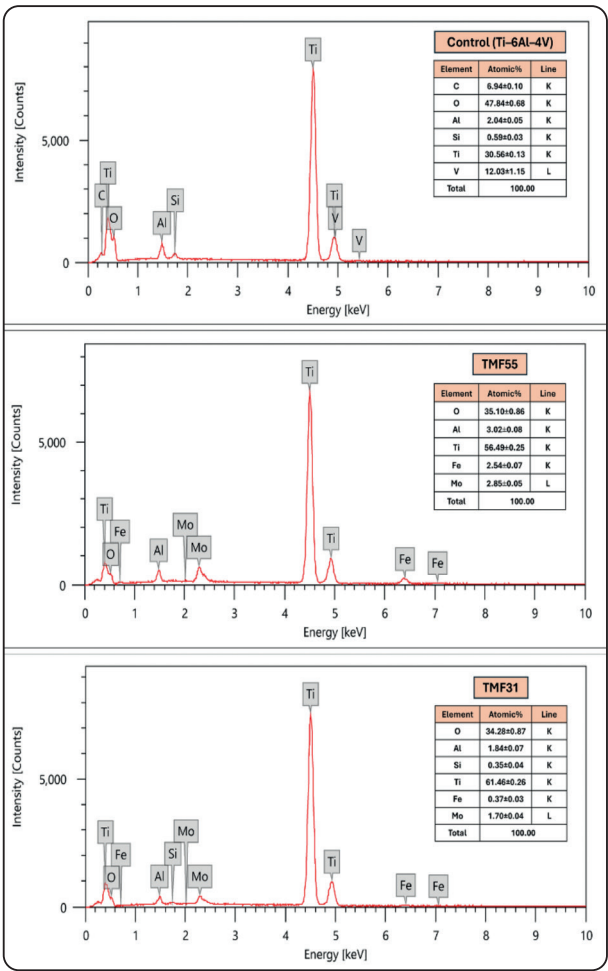

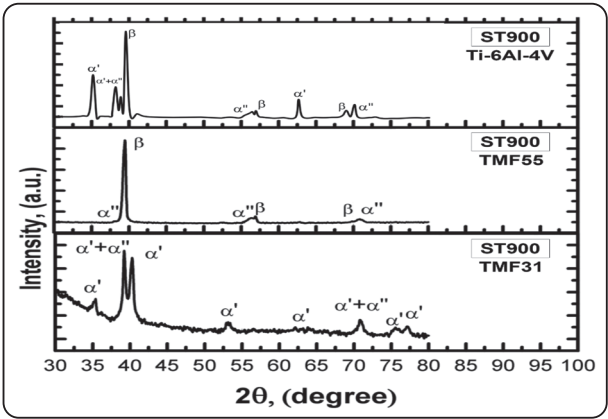Fig. (1) EDX spectrums of the control (Ti–6Al–4V), TMF55 and TMF31 implant alloys

Fig. (2) X-ray diffraction patterns of control (Ti-6Al-4V), TMF55 and TMF31 implant alloys in solid solution treatment at 900°C/1hr

The mean values of Young's moduli for the studied groups are shown in Table [2]. The control group recorded the highest mean Young's modulus value of 110 GPa with a standard deviation (SD) 0.63. On the other hand, there was a significant decrease in the mean Young's modulus values for the two test implant alloys, which were 82 GPa with SD 0.89 for TMF55 and 83.17 GPa with SD 0.75 for TMF31 (P<0.0001). No significant difference was detected between the mean Young's modulus values of the two test groups (P=0.06).

TABLE (2) Comparison of Young's moduli among the three studied groups

	Control (Ti-6Al-4V) Implant Alloy (n=6)	TMF55 Implant Alloy (n=6)	TMF31 Implant Alloy (n=6)
Range	109-111	81-83	82-84
Mean	110.00	82.00	83.17
S.D.	0.63	0.89	0.75
ANOVA (F value)	2556.32		
P value	<0.0001*		
P1	<0.0001*		
P2	<0.0001*		
P3	0.06		

P was significant if ≤0.05

*Significant difference at level 0.05

P1 comparison between control group and TMF55 group

P2 comparison between control group and TMF31 group

P3 comparison between TMF55 group and TMF31 group

The cytotoxicity-Biocompatibility outcomes

The cytotoxicity test was employed to assess the biocompatibility of the control and designed alloys TMF55 and TMF31. Figure [3. A-C] illustrates the MC3T3-E1 cells morphologies and cell adhesions of control (Ti-6Al-4V), TMF55, and TMF31 implant alloys, as determined by the direct cytotoxicity test conducted for 6 hours using the CCK-8 assay. This short culture period was used to examine the cell size and the shape index of the attached cells. The TMF31 alloy recorded the largest cell size and the highest shape index values compared to the other alloys (TMF55 and control). The cell size and shape index of the control alloy were close to those of the TMF31 alloy. Conversely, the TMF55 alloy exhibited the smallest cell size, and the lowest shape index compared to both the control and TMF31 alloys.

Cell viability, indicated by the number of attached MC3T3-E1 cells, was assessed for both the control and test implant alloys using ImageJ software after 6-hour and after 7 days incubation. The results are displayed in Table [3] and Figure [4]. Regarding the outcomes after 6-hours incubation, the TMF55 alloy recorded the lowest mean value of attached MC3T3-E1 cells 51.83 with SD 0.75. Both the control and TMF31 alloys showed a significant increase in the mean number of MC3T3-E1 cells attached, with values of 98 with SD 0.89 and 101.17 with SD 1.17 (P <0.0001), respectively. Furthermore, a statistically significant difference

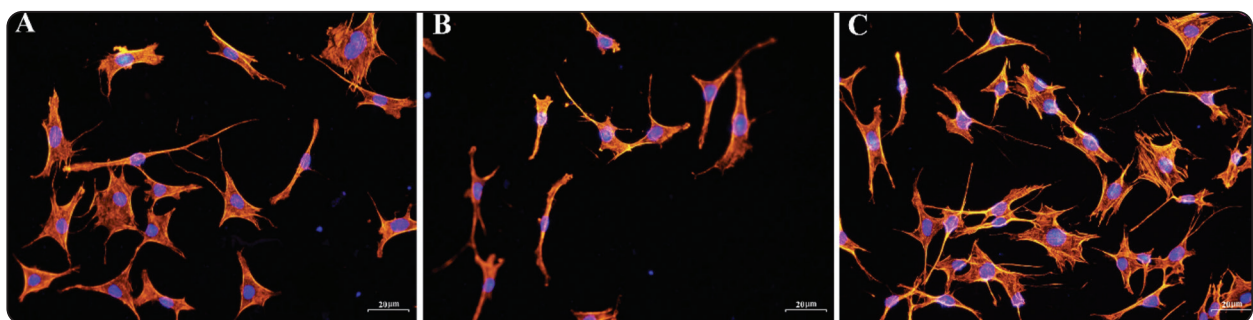Fig. (3) Cytoskeletal morphology of MC3T3-E1 cells cultivated for 6 h on: (A) control (Ti-6Al-4V), (B) TMF55, and (C) TMF31implant alloys

was observed in the number of attached MC3T3-E1 cells between the control and TMF31 alloys (P=0.0001). The cell viability of MC3T3-E1 cells seeded on control, TMF55 and TMF31 alloys after 7 days incubation revealed an active proliferation rate represented by extensive cell spreading with numerous nuclei, comparable results were observed after a 7-day incubation period. The TMF31 alloy showed the highest cell viability, with a mean of 732.17 attached MC3T3-E1 cells (SD = 2.48), followed by the control alloy with a mean of 728.17 attached cells (SD = 2.56). A statistically significant difference was detected between the two alloys (P = 0.04). The TMF55 alloy disclosed the significantly lowest mean number of attached MC3T3-E1 cells 389 with SD 2.28 (P <0.0001). A comparison of cell viability between 6-hour and 7-day incubation periods revealed a statistically significant increase in both the control and the two test alloys.

Histological and immunohistochemical observations

The histological observations at the two-weeks healing period for the control group illustrated that bone segments facing the implant interface were separated by relatively wider interruption than contact regions. The adjacent osseous tissue appeared to be in a state of relative immaturity, and an evident cementing line could be seen in all sections bordering the assumed line of contact between the bone and the implant. However, the two-weeks histological picture in association with TMF55 implants was unsatisfactory. The bone segments adjacent to the implant space displayed significant disorganization, diminished volume and were widely separated by interruption areas directly contacting the implant without an intervening cementing line along most of the interface. The bone of the interface exhibited brownish metallic color and poor quality, with separation of its different lamellae and accommodation of numerous osteocyte spaces. On the contrary, adequate histological outcomes were noted following a two-week healing

TABLE (3) Comparison of cell viability based on attached MC3T3-E1 cells number among the three studied groups after 6 hours and 7 days incubation periods

	Control (Ti-6Al-4V) Implant Alloy (n=6)	TMF55 Implant Alloy (n=6)	TMF31 Implant Alloy (n=6)
After 6 hours			
Range	97-99	51-53	100-103
Mean	98.00	51.83	101.17
S.D.	0.89	0.75	1.17
ANOVA (F value)	5021.52		
P value	<0.0001*		
P1	<0.0001*		
P2	0.0001*		
P3	<0.0001*		
After 7 days			
Range	725-732	386-392	729-736
Mean	728.17	389.00	732.17
S.D.	2.56	2.28	2.48
ANOVA (F value)	38946.48		
P value	<0.0001*		
P1	<0.0001*		
P2	0.04*		
P3	<0.0001*		

P was significant if ≤0.05
*Significant difference at level 0.05
P1 comparison between control group and TMF55 group
P2 comparison between control group and TMF31 group
P3 comparison between TMF55 group and TMF31 group

period for TMF31 implants. The bone facing the implant site displayed enhanced organization with fewer osteocytes compared to the previous two groups. The contact segments appeared broader, and a distinct cementing line could be traced consistently across the entire interface without any discontinuities. The bone trabeculae adjacent to the implant space, as well as the deeper ones, were well-vascularized and densely packed, creating a robust insertion tissue for the implant [Figure 5. A-C]. Similar immunohistochemical results regarding osteopontin localization were observed following a two-week healing period for both the control and test groups. Osteopontin expression at
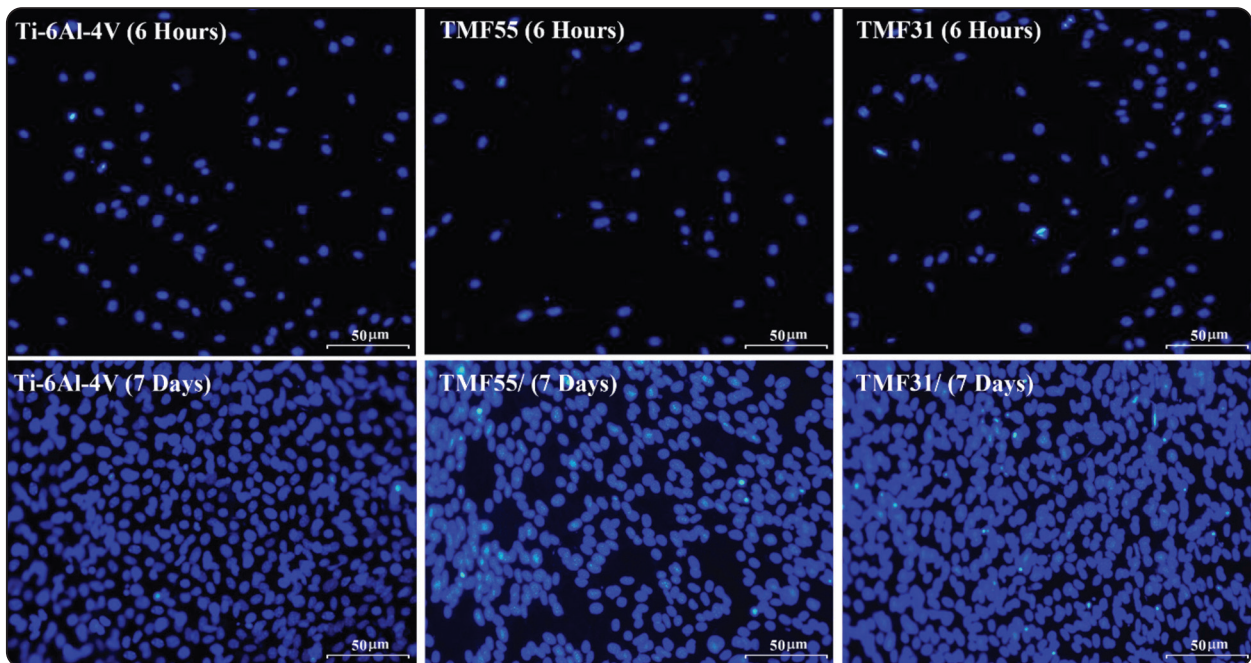
Fig. (4) Cell viability, determined by the number of attached MC3T3-E1 on the control (Ti-6Al-4V), TMF55, and TMF31 implant alloys following incubation periods of 6 hours and 7 days.

the cementing line showed strong and comparable levels in both the control and TMF31 groups. This was evidenced by deep brown staining along the cementing line, accentuating its significance in the initial mineralization process for implant osseointegration. Conversely, the expression associated with TMF55 implants exhibited a weaker immune response [Figure 6. A-C]. Concerning the histological observations following the six-week healing period for control and test groups, it was noted that the control implants showed appropriate osseointegration features signified by broader segments of bone contact to the assumed implant outline compared to the two-week observation period, with subsequent less interruption areas. Additionally, the bone at the interface demonstrated improved organization, greater thickness, and better continuity with the deeper bone into which the implant was inserted. This deeper bone exhibited enhanced blood supply and cellular activity. Notably, a continuous cementing line was prominently observed in almost all sections of this group. However, the bone adjacent to the assumed TMF55

implant surfaces displayed poor osseointegration attributes characterized by a distinctive disorganized appearance reminiscent of that observed during the initial two-week observation period. Although the frequency of contact segments was slightly higher compared to the two-week period, the interface bone exhibited a brownish metallic discoloration. The predominant bone type forming the interface was the woven immature variety, and even the few areas of lamellated bone showed splitting of their individual lamellae. Remarkably, no cementing line was observed along the entire length of the presumed interface. It is worth noting that the most favorable histological findings pointing exceptional peri-implant osseointegration were observed in conjunction with TMF31 implants. The assumed bone implant interface consisted of an almost continuous contact line with very few interruption segments. Additionally, in both scenarios, the interface was bordered by a continuous cementing line. Moreover, the deeper bone demonstrated remarkably high density and excellent organization [Figure 7.A-C].
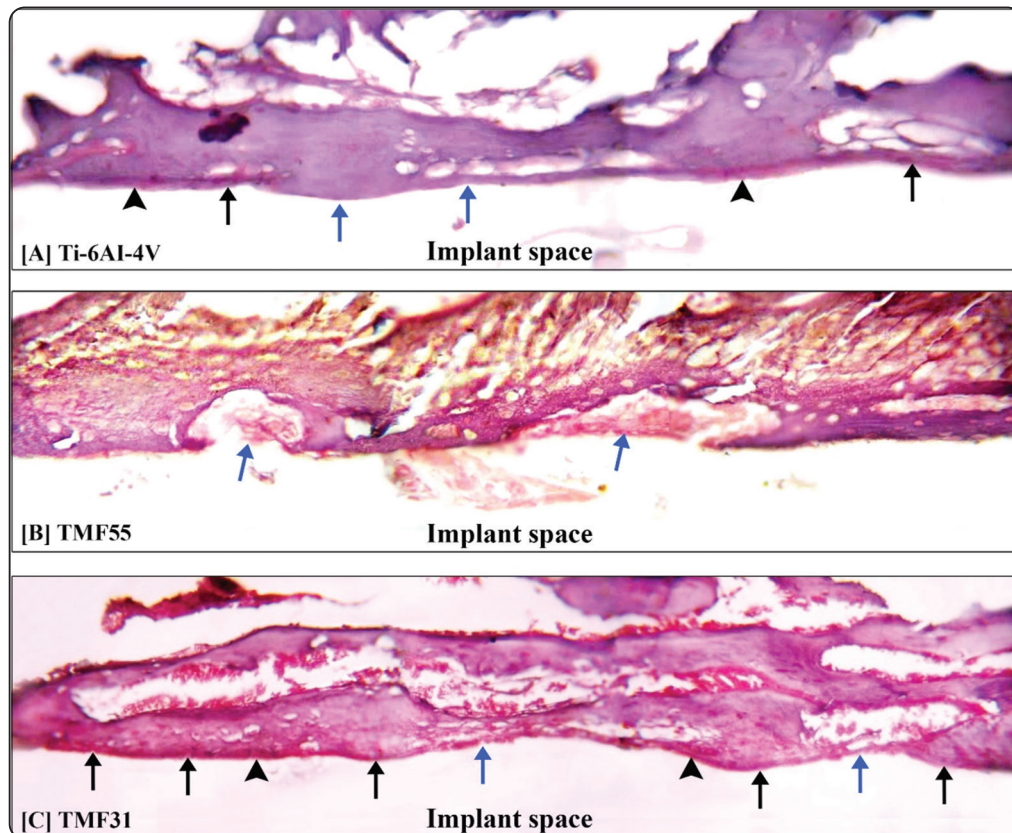
Fig. (5) A–C: Light micrographs (LM), H&E, × 400 showed the peri-implant osseointegration after the two-week healing period for the three studied groups. The control (Ti-6Al-4V) titanium implant bone interface revealed broad areas of direct bone contact (black arrows), along with intermittent interruptions (blue arrows). Additionally, there was an obvious continuity along the cementing line bordering this interface, alongside the determination of good bone quality (arrowheads), (A). The bone implant interface of the TMF55 titanium implants exhibited substantial regions of interruption with lack of cementing line along this interface (blue arrows). Moreover, there was extremely disorganized bone tissue with a discernible brownish metallic hue, (B). Adequate osseointegration features were evidenced along the bone implant interface of TMF31 titanium implants, as demonstrated by the observation of expansive bone segments in contact with the presumed implant surface, surpassing those seen in the previous two groups (black arrows). The discontinuous regions appear to recede from the boundary of bone contact (blue arrows). Notably, a continuous cementing line (arrowheads) and large prominent blood vessels among the bone trabeculae with their few contents of osteocytes are detectable, (C).
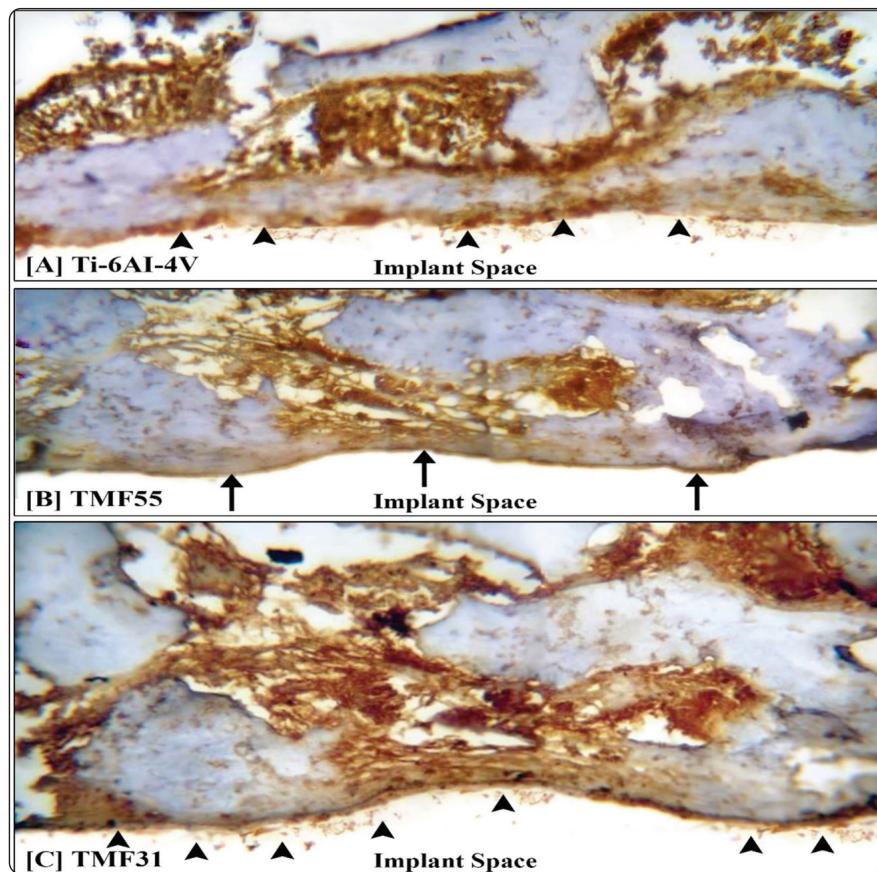
Fig. (6) A–C: Light micrographs (LM), × 400 depict the immunohistochemical findings of osteopontin expression following the two-week healing period for the three investigated groups. Strong osteopontin expression was detected in the cementing line adjacent to the presumed implant surface (arrowheads) for the control (Ti-6Al-4V) (A) and TMF31 (C) implants. Conversely, weak osteopontin expression in the cementing line adjacent to the TMF55 presumed implant surfaces was observed (arrows) (B).

Histomorphometric findings (BIC%)

Stereomicroscopic images of the histomorphometric analysis were captured to screen the Bone-to-Implant Contact percentage (BIC%) of each studied group following both the two-week and six-week healing intervals, as depicted in Figure [8]. The histomorphometric outcomes represented by the calculated mean values of Bone-to-Implant Contact (BIC%) for the three studied groups at both the two- and six-weeks healing periods are summarized in Table [4]. Following the two-week period,

it was observed that the TMF55 titanium implant surfaces exhibited the lowest mean BIC% value 28.83 with SD ±1.17. Subsequently, a significant increase in the BIC% mean value was noted for both the control (Ti-6Al-4V) and TMF31 titanium implant surfaces, measured as 45.33 with SD ±1.63 and 49.17 with SD ±0.98 respectively. These results indicated a statistically significant increase in BIC% from the TMF55 implant group to both the control (P=0.001) and TMF31 groups (P=0.001). However, there was no statistically significant difference
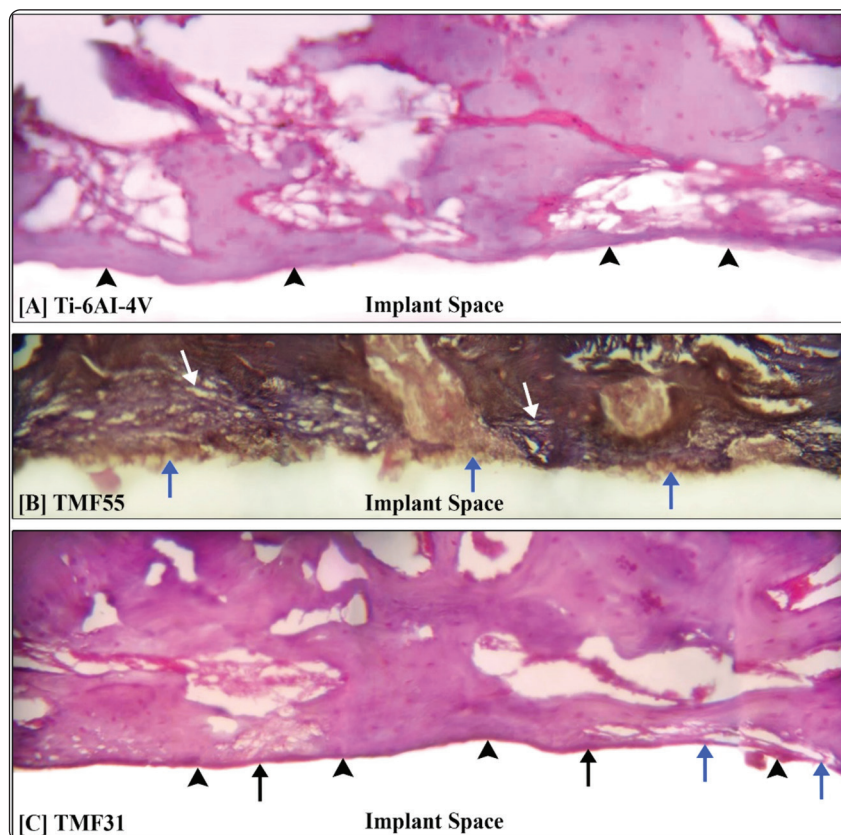
Fig. (7) A–C: Light micrographs (LM), H&E, × 400 showed the peri-implant osseointegration after the six-week healing period for the three studied groups. (A) The interface of the control (Ti-6Al-4V) implant surfaces exhibited remarkable osseointegration appearances, characterized by excellent bone quality, robust blood supply, and a clearly discernible cementing line along the implant interface, devoid of any interruption zones, (arrowheads). The osseointegration of TMF55 peri-implants revealed obviously poor and immature bone quality adjacent to the implant space, characterized by a brownish discoloration, lamellar splitting (white arrows), and an absence of a distinct cementing line (blue arrows). Evidently, the extent of presumed bone-implant contact is notably limited, (B). The TMF31 implants exhibited approximately complete contact between the presumed implant interface and the surrounding bone (black arrows), with minimal interruption areas (blue arrows) and a distinct cementing line along this interface (arrowheads). Noteworthy is the thickness of the trabeculae of the adjacent bone and their interconnectivity, (C).

in BIC% between the control and TMF31 groups (P=0.107) during this period. Similar results were found during the six-week peri-implant healing period for both control and test groups. The mean BIC% value was 81.50 with SD ±1.38 for the control group, and 55.17 with SD ±0.98, 86.67 with SD ±1.03 for TMF55, and TMF31 groups respectively. Again, a statistically significant increase in BIC% mean value was observed from the TMF55 implants to both the control (P=0.001) and TMF31 implant groups (P=0.001). Furthermore, there was no statistically significant difference in BIC% mean values between the control and TMF31 groups (P=0.231) at this healing stage.
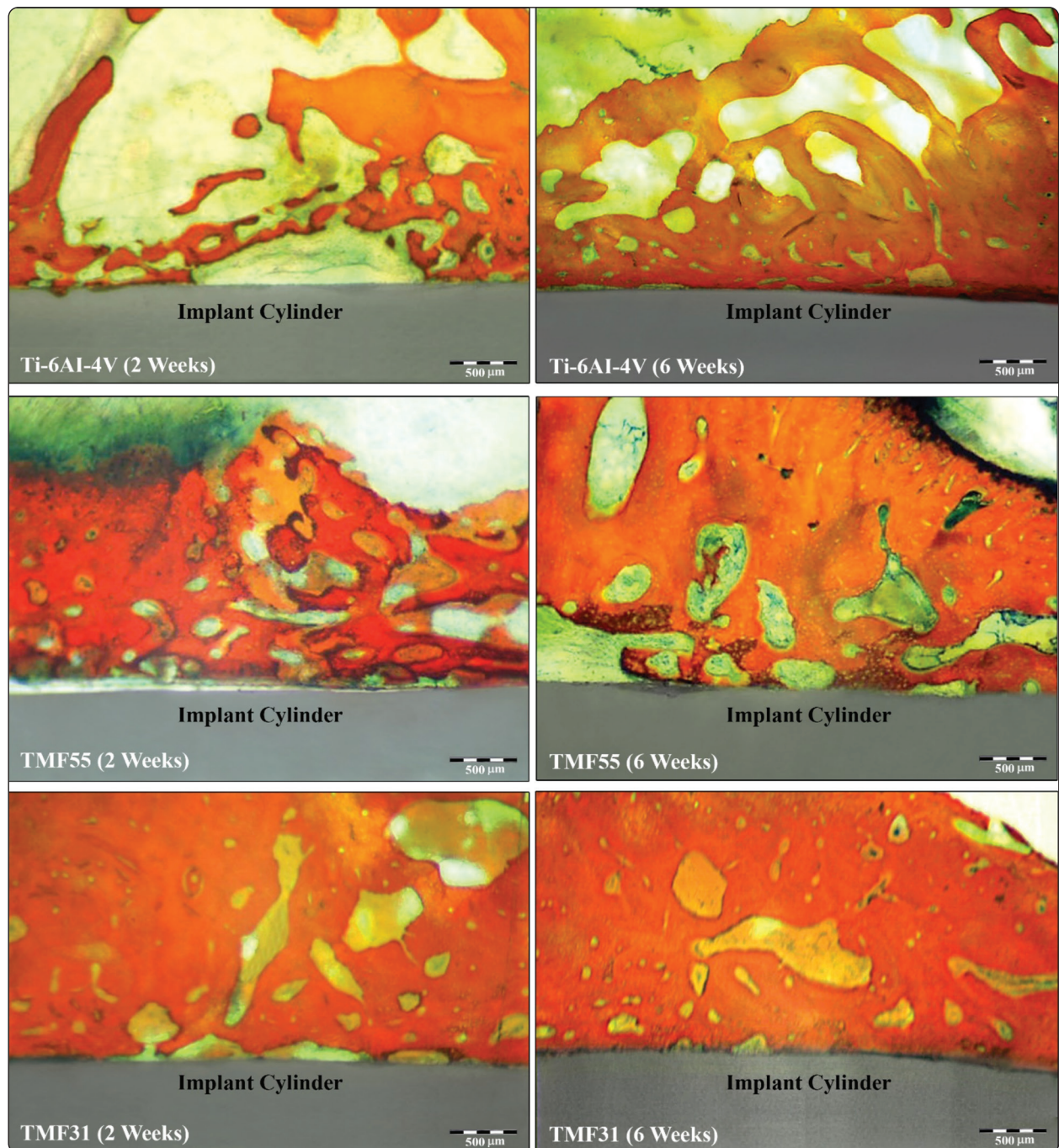
Fig. (8) Stereomicroscopic images (X: 11 × 10) show the bone-implant contact (BIC%) for the control group (Ti-6Al-4V) and the TMF55 and TMF31 implant groups after 2-week and 6-week healing periods. The contact line between the newly formed bone and the implant surface in each group indicates the BIC%.

TABLE (4) Comparison of BIC% among the three studied groups at both two-week and six-week healing intervals.

	Control (Ti-6Al-4V) Implant Alloy (n=6)	TMF55 Implant Alloy (n=6)	TMF31 Implant Alloy (n=6)
After 2 weeks			
Range	43-47	27-30	48-50
Mean	45.33	28.83	49.17
S.D.	1.63	1.17	0.98
ANOVA		25.85	
P value		0.001*	
P1		0.001*	
P2		0.11	
P3		0.001*	
After 6 weeks			
Range	80-84	54-56	85-88
Mean	81.50	55.17	86.67
S.D.	1.38	0.98	1.03
ANOVA		19.85	
P value		0.001*	
P1		0.001*	
P2		0.23	
P3		0.001*	

P was significant if ≤ 0.05   ** Significant difference at level 0.05*
P1 comparison between control group and TMF55 group   *P2 comparison between control group and TMF31 group*
P3 comparison between TMF55 and TMF31 group

DISCUSSION

Titanium is the premier choice for dental implant alloys owing to its superior mechanical characteristics, low density, and high biocompatibility with bone tissue. The main alloy utilized is commercially pure titanium (cpTi). This metal is produced in four different grades, determined by its purity and the oxygen content introduced during processing. These grades differ in ductility, strength, and corrosion resistance [20].

Grade V titanium alloy (Ti-6Al-4V) is commonly used in orthopedics for its exceptional strength and lower Young's modulus. Although it is also employed in dentistry as a dental implant alloy and has shown biological compatibility, this alloy releases both aluminum and vanadium, which may pose potential biological risks [21]. Moreover, grade V titanium alloy exhibits negligible corrosion and induces minimal systemic effects in a minority of patients. Biomechanically, it is highly suitable for its intended application, with sustained high clinical survival rates over extended service periods. Consequently, opportunities for enhancement are limited. Yet, there has been research interest in the development of novel alloys for dental implant use. The predominant strategy involves eliminating biologically harmful elements, particularly vanadium, and optimizing the modulus to closely align with that of bone tissue [22].

Modern compositions of titanium alloys include non-toxic elements such as Mo, Nb, Fe, Zr, Ta, and Sn. Compared to traditional metallic biomaterials like Ti-6Al-4V, Co-Cr–Mo alloys, and 316L stainless steel, β-Ti alloys offer a lower modulus. Research efforts in β-Ti alloy production concentrate on three main aspects: designing alloy compositions, thermo-mechanical processing, and performance evaluation. Achieving a low elastic modulus is a primary objective in designing these alloy compositions [23].

Currently, a significant array of β-type titanium alloys serves as metallic biomaterials in various biomedical implants including artificial hip joints, heart valves, dental applications, and more. Historically, Co–Cr-based alloys and (α+β)-type titanium alloys were favored over other biomedical alloys. However, β-type titanium alloys have emerged as the preferred choice due to their ability to achieve high strength levels and exceptional fatigue resistance [20]. Kent et al. [24] investigated the mechanical characteristics of β-type titanium alloys and observed that cold-rolled specimens exhibit strengths exceeding 900 MPa. Niinomi et al. [25] conducted research on the aging behavior of β-type titanium alloys at 573 K, discovering that their fatigue resistance improves while maintaining a modulus below 80 GPa post-aging. Therefore, β-type titanium alloys can achieve notable fatigue resistance through suitable thermo-mechanical treatments. In achieving the targeted mechanical properties of β-type titanium alloys, the incorporation of alloying elements plays a pivotal role. Ehtemam-Haghighi et al. [26] demonstrated that the addition of iron (Fe) reduces the formation of α'' martensite, thereby enhancing the stability of the β phase within titanium alloys. This increase in Fe content correlates directly with improved alloy strength. Consequently, the strategic design of new β-type titanium alloys, leveraging such elements, offers a viable and economical means to attain controllable mechanical properties. In a similar manner, substituting vanadium (V) with

molybdenum (Mo) in titanium alloys used for dental implants can lead to improved biocompatibility. Alloys containing Mo have demonstrated decreased ion release, enhanced resistance to corrosion, and improved mechanical properties, all while maintaining favorable acceptance by biological tissues. On the other hand, thermo-mechanical processing and heat treatment offer effective means to alter the β-type titanium alloys microstructures and customize their mechanical properties. Liang et al. [27] developed β-type titanium alloy, Ti–31Nb–6Zr–5Mo, utilizing the d-electron method in a vacuum non-consumable furnace. They conducted solution treatment following hot rolling, both with and without subsequent aging treatment. During solution treatment at 800 °C for 30 minutes, the fibrous grains rich in Nb, which were generated by hot rolling, dissolved back into the alloy. This process resulted in a homogeneous distribution of alloying elements within Ti–31Nb–6Zr–5Mo. Subsequently, aging treatment at 300 °C for 2 hours redistributed the Nb element to form regions with enriched and depleted β phases. Remarkably, both solution-treated and aging-treated samples exhibited identical crystal structures.

Based on the previous research findings, the (β)-type Ti–4.7Mo–4.5Fe (TMF55) alloy and (α+β)-type Ti–3Mo–0.5Fe (TMF31) bio-innovative titanium implant alloys were designed throughout this research to replace the V ions found in Grade V (Ti-6Al-4V) titanium implant alloys, which were used as the control. This substitution involved incorporating Fe and Mo as β-stabilizing elements, with the goal of enhancing biocompatibility, reducing the elastic modulus, and improving osseous bioactive performance. For in vitro testing, 90 discs (8mmx3mm) were prepared and equally divided into three groups, (n=30): control (Ti-6Al-4V) and two designed TMF55 and TMF31 titanium alloys. Analysis of EDX spectra and atomic percentages of V, Fe, and Mo in the three implant alloys confirmed the successful replacement of V with Fe and Mo. Vanadium (V) was not detected in

the two designed alloys. Furthermore, statistically significant increase was observed in the mean atomic percentages of Fe, from 0.36 in TMF31 to 2.51 in TMF55 (P < 0.0001), and Mo, from 1.70 in TMF31 to 2.83 in TMF55 (P < 0.0001). The higher atomic percentages of Fe and Mo β-stabilizer elements in the TMF55 titanium alloy compared to TMF31 indicate the achievable engineering of (β)-type Ti–4.7Mo–4.5Fe (TMF55) and (α+β)-type Ti–3Mo–0.5Fe (TMF31) vanadium free implant alloys. This accomplishment positions them as smart bioactive, cost-effective, and biocompatible alternatives to Ti-6Al-4V titanium implant alloys. These outcomes were correlated with the phase identification and microstructure XRD patterns of the control and both developed implant alloys. In the TMF55 alloy, the β-phase is clearly dominant, with a minor presence of orthorhombic α″ martensite. The inclusion of Fe and Mo in the alloy effectively stabilizes the β-phase even after solution treatment. Conversely, following ST900 treatment of the TMF31 alloy, the predominant phase observed is solely the α″ (orthorhombic martensite) phase, while the β one was irrelevant. This distinction arises from the specific compositions of the two implant alloys in this study. The (α+β)-type Ti–3Mo–0.5Fe (TMF31) alloy was formulated with lower concentrations of Fe and Mo to promote a martensitic structure. In contrast, the other (β)-type Ti–4.7Mo–4.5Fe (TMF55) alloy contained higher amounts of these elements, strategically designed to stabilize a single β-phase structure. Regarding the XRD pattern of the control (Ti-6Al-4V) implant alloy after ST900 treatment, the observed characteristic peaks indicate the detection of both α and β phases.

Elbanna et al. [28] conducted an analysis of the elemental composition of TMF31 (Ti–3 at. % Mo–1 at. % Fe) and TMF55 (Ti–5 at. % Mo–5 at. % Fe) alloys using energy dispersive X-ray spectroscopy (EDX) before and after anodization. The atomic percentages of Ti, Mo, and Fe were noted to vary between the samples. Post-anodization, EDX results revealed peaks for Ti, Mo, Fe, and O only,

indicating the absence of any foreign elements and confirming the successful formation of high-purity Ti–Mo–Fe–O nanotubes. Importantly, no complete dealloying of Mo and Fe was observed after anodization. Moreover, it was found that increasing the anodization time caused faster partial dealloying in TMF31 samples compared to TMF55, highlighting the differences in atomic percentages between the two samples. Otherwise, Mohan et al. [29] reported that the crystal structures of Ti12Mo6Zr alloys are significantly influenced by the addition of Fe. The Ti12Mo6Zr alloy primarily consists of the α′ and β phases, with a composition of 50.61% α-phase and 49.39% β-phase. However, when 3 wt.% Fe or more is added, the β phase is almost entirely retained, exhibiting a BCC crystal structure, with only 1.08% α-phase and 98.92% β-phase. This retention is attributed to the well-known stabilizing effect of Fe on the β phase.

The Young's modulus is a crucial property influencing the biomechanical interaction between bone and implant. Lowering the elastic modulus helps mitigate bone atrophy and enhances stress distribution at the implant-bone interface. The elastic modulus should ideally closely match that of bone to minimize the phenomenon known as "stress shielding," which has been linked to osteoporosis and bone resorption near the implant site [30].

The results of the current study show that the mean Young's modulus for the control implant alloy was 110 GPa. In contrast, both designed implant alloys demonstrated a significant reduction in mean Young's modulus values of 82 GPa with (β)-type TMF55 and 83.17 GPa for (α+β)-type TMF31 measuring (P<0.0001). There was no statistically significant difference observed between the mean Young's modulus values of the two test groups (P=0.06). This could be attributed to the behavior where the elastic modulus initially increases with an increase in β content but then sharply decreases at higher concentrations. Typically, β-stabilizers at lower concentrations result in α + β alloys, which exhibit higher elastic modulus values due to the

presence of the α phase. However, as the β phase concentration rises, the α phase diminishes in the alloy structure, leading to a reduction in elastic modulus [31].

Efforts to enhance mechanical properties of hip prosthesis materials have included various strategies. For example, incorporating elements such as iron and niobium into titanium-aluminum alloys has led to increased dynamic stiffness and reduced elastic modulus. As a result, alloys like Ti5Al2.5Fe and Ti6Al7Nb achieve improved stress distribution between the implant and bone tissue along with a lower Young's modulus. Another category of titanium alloys used in orthopedic applications is β-Ti alloys, which incorporate molybdenum to stabilize the β phase of titanium at room temperature [32].

Cytotoxicity testing was conducted to evaluate the biocompatibility of the control and both designed implant alloys TMF55 and TMF31 using the CCK-8 assay. A larger cell size with a high shape index indicates extensive spreading of cells on the sample surface, suggesting healthy growth of the seeded cells. The TMF31 alloy demonstrated the largest cell dimensions and highest shape index values among the alloys studied (TMF55 and control). The cell size and shape index of the control alloy closely approximated those of the TMF31 alloy. In contrast, the TMF55 alloy demonstrated the smallest cell size and lowest shape index relative to both the control and TMF31 alloys. These results indicate that TMF31 and control alloys considerably enhanced the seeding and growth of MC3T3-E1 cells compared to TMF55 alloy.

Cell viability, assessed by counting the number of attached MC3T3-E1 cells, was evaluated for both the control and test implant alloys using ImageJ software after 6 hours and 7 days of incubation. Similar results were observed after both the 6-hour and 7-day incubation periods. The TMF55 alloy exhibited a statistically significant decrease in the mean number of attached MC3T3-E1 cells compared

to both the control and TMF31 implant alloys. Furthermore, a statistically significant difference was noted between the control and TMF31 implant alloys after both incubation periods. These findings indicate that TMF31 significantly enhanced cell viability, followed by the control implant alloy, while the TMF55 implant alloy exhibited the least cell viability. This suggests that TMF31 and control implant alloys possess considerable biocompatibility.

Numerous studies have investigated the cytotoxicity of various titanium alloys. Ti-6Al-4V has been found to exhibit cytotoxicity corresponding pure titanium metal, despite containing aluminum and vanadium. Other alloying elements such as iron, molybdenum, niobium, zirconium, and tantalum have also shown acceptable cytotoxicity profiles in MTT assays. However, copper has been noted to significantly increase cytotoxicity. Studies have established that low cytotoxicity is associated with the ability of cells to adhere to metal surfaces and maintain functionality. This low cytotoxicity forms the basis for other favorable biological properties of titanium alloys, including biocompatibility and osseointegration [20].

According to Cao et al. [33], the optical density (OD) of MC3T3-E1 cells was assessed using the MTT assay after 1, 3, and 5 days of incubation on cp-Ti and Ti–Cu samples. Initially, there was no significant difference in OD values between cp-Ti and Ti–Cu samples on the first day, nor among different Ti–Cu samples. By the third day, the OD values of Ti–Cu samples were notably lower than those of cp-Ti, and Ti–Cu samples treated with anodic oxidation (AO) exhibited even lower OD values compared to untreated Ti–Cu samples, though there was no distinction among AO-treated Ti–Cu samples. However, the OD values of Ti–Cu samples were significantly higher than those of cp-Ti on the fifth day, with no variability observed among the OD values of different Ti–Cu samples.

It is noteworthy that the in vitro findings of this study confirmed the successful substitution of V in control Grade V (Ti-6Al-4V) titanium alloy with Fe and Mo β-stabilizing elements, resulting in the production of (β)-type Ti–4.7Mo–4.5Fe (TMF55) and (α+β)-type Ti–3Mo–0.5Fe (TMF31) bio-innovative titanium implant alloys free of vanadium. These designed alloys exhibited a lower Young's modulus compared to the control alloy. In terms of biocompatibility, TMF31 demonstrated biocompatibility analogous to the control Ti-6Al-4V implant alloy, whereas TMF55 showed lower biocompatibility properties. Therefore, conducting an in vivo animal study phase is crucial to verify the biocompatibility and bioactive osseointegration of TMF55 and TMF31 titanium alloys in contrast to the control (Ti-6Al-4V) implant alloys.

The in vivo animal study was conducted on six-month-old male line V Spain white rabbits, each weighing 3 kg. These rabbits were divided randomly into three groups corresponding to the implant groups: the control group (Ti–6Al–4V), TMF55 and TMF31 test groups. Histological observations of both the control (Ti-6Al-4V) and TMF31 titanium implant alloys after two and six weeks revealed satisfactory bioactive peri-implant osteointegration. This was marked by the appropriate dispersion of bone contact segments along the bone-implant interface, with evident cementing line continuity and newly formed bone of high quality and maturity. Both implant groups showed strong osteopontin expression in the cementing line adjacent to the implant surfaces. On the other hand, TMF55 titanium implant surfaces demonstrated poorer osteointegration, characterized by lack of bone contact areas and absence of cementing line across the bone-implant interface. Also, the bone facing the implant surfaces appeared of poor quality, highly disorganized, and exhibited a brown metallic color along with a weak osteopontin expression. Comparable histomorphometric results, reflected by the calculated Bone-to-Implant Contact (BIC%) percentages for the studied titanium implant alloys, supported the previous histological and immunohistochemical findings. TMF55 implant surfaces showed the lowest mean BIC%, whereas control and TMF31 implants demonstrated significantly higher mean BIC% values.

It is remarkable that the in vitro cytotoxicity and biocompatibility results of the three titanium implant alloys were validated by osteogenic bioactivity, osteopontin expression, and BIC% histomorphometry. Compared to the control (Ti-6Al-4V) dental implant alloy, the TMF31 titanium implant alloy showed competent biocompatibility, with no inhibition of cell viability or growth, and excellent peri-implant osseointegration bioactivity. In contrast, the engineered TMF55 titanium alloy displayed poor biocompatibility and inferior osteogenic bioactivity around implant surfaces. This could be attributed to the elemental composition of the designed alloys. In the TMF31 titanium alloy, replacing V with low concentrations of Fe and the highly biocompatible alloying element Mo, along with the stable molybdenum oxide layer on the alloy surface, inhibits metal ion release [34]. On the other hand, the high atomic percentage of Fe in the TMF55 titanium alloy, although with the high concentration of Mo may be responsible for its cytotoxic effects, poor biocompatibility, deficient osteointegration, and the brownish discoloration of the bone formed along the bone-implant interface.

These results of the TMF31 dental implant alloy agreed with those of Ti-6Al-7Nb multi-component titanium alloy that has garnered attention for biomedical implant applications. This alloy is immensely used for dental implant fabrication. As an α+β alloy initially developed for orthopedics, it possesses superior mechanical properties compared to commercially pure titanium (cpTi). Ti-6Al-7Nb is corrosion resistant with acceptable biological properties, mainly due to the absence of vanadium. In terms of biological responses, Ti-6Al-7Nb behaves similarly to cpTi. Implantation of Ti-6Al-7Nb for a short time illicit a transient inflammatory response as cpTi, leading to improved biocompatibility.

Ti-6Al-7Nb has shown better osteoblast-like cell spreading than cpTi and demonstrates good osseointegration in animal models such as dogs [35].

Additionally, a preclinical study compared the bone contact, density, and neoformation between Ti-Al16-V4 titanium (Ti) implants with SLA treated surfaces and those modified with carboxyethylphosphonic acid (CEPA) and bone morphogenetic protein 2 (BMP-2) after a 4-week implantation period in minipig tibia. Ti-Al16-V4 dental implant surfaces altered with CEPA and BMP-2 demonstrated an improved peri-implant osseointegration [36].

Throughout this study, the null hypothesis, which stated no significant differences in biocompatibility, cytotoxicity, and osseointegration bioactivity among the TMF55 alloy, TMF31 alloy, and the conventional Ti–6Al–4V (Grade V) alloy for dental implant applications, was thoroughly examined. The comparative analysis involving laboratory testing, cytotoxicity evaluations, and experimental histological assessments revealed significant differences among the alloys. The TMF31 alloys demonstrated superior biocompatibility and osseointegration bioactivity, whereas TMF55 alloy showed poor performance compared to the conventional Ti–6Al–4V (Grade V) alloy. Consequently, the null hypothesis was rejected.

CONCLUSION

Within the limitations of this study, it could be concluded that two vanadium-free titanium implant alloys were successfully engineered. This was achieved by replacing vanadium (V) in the Grade V (Ti-6Al-4V) alloy with iron (Fe) and molybdenum (Mo) in different concentrations, resulting in the development of the (β)-type Ti-4.7Mo-4.5Fe (TMF55) and ($\alpha+\beta$)-type Ti-3Mo-0.5Fe (TMF31) alloys. These designed alloys are low-cost and possess a lower elastic modulus, thus reducing peri-implant stress shielding. The control (Ti-6Al-4V) and TMF31 titanium alloys displayed good cell viability after 6 hours and 7 days incubation as well as

excellent biocompatible assay along with low cytotoxicity, while the TMF55 alloy exhibited opposite characteristics. Superior peri-implant osseointegration features were observed around the control (Ti-6Al-4V) and TMF31 implant surfaces, with significantly higher BIC % values compared to the TMF55 alloy implant surfaces. Therefore, the developed TMF31 titanium implant alloy demonstrates significant potential for bioactive osteogenic activity and excellent biocompatibility. This positions it as a promising bio-innovative, low-cost competitor to the commonly used Grade V (Ti–6Al–4V) titanium alloy in dental implants. Conversely, the fabricated TMF55 alloy exhibits inadequate osseointegration capabilities and poor biocompatibility, rendering it unsuitable for biomedical applications, particularly in dental implantology.

Ethics approval

The in vitro cell viability and biocompatibility, along with the in vivo animal experimentation phase, were conducted in accordance with the approved ethics guidelines established by the Institutional Animal Care and Use Committee (ALEXUIACUC) at Alexandria University, under protocol number 112310153.

Consent for publication

Not applicable.

Availability of data and materials

The datasets and analyses utilized in this study are available from the corresponding author upon reasonable request. Data is provided within the manuscript or supplementary information files.

Competing interests

The authors declare that they have no competing interests.

Authors' contributions

All authors contributed to the conceptualization and design of the study. Alloy design and specimen preparation were carried out by YA and MG. In vitro characterization, data acquisition, and statistical analysis were performed by DW, YA, SK, and MG. Figures 1,2 was prepared by DM, and figures 3,4 was prepared by YA and MG. The in vivo phase, along with histological and histomorphometric evaluations, was conducted by DM and SS. Figures 5,6, and 7 were prepared by SS, and figure 8 was prepared by DM. Drafting the manuscript and its initial preparation was conducted by DM. All authors critically reviewed, revised, and approved the final version of the manuscript.

REFERENCES

1. Sanz M, Noguerol B, Sanz-Sanchez I, Hammerle CH, Schliephake H, Renouard F, Sicilia A, Steering Committee, Cordaro L, Jung R, Klinge B. European Association for Osseointegration Delphi study on the trends in Implant Dentistry in Europe for the year 2030. Clinical oral implants research. 2019 May;30(5):476-86. https://doi.org/10.1111/clr.13431

2. Huang X, Bai J, Liu X, Meng Z, Shang Y, Jiao T, Chen G, Deng J. Scientometric analysis of dental implant research over the past 10 years and future research trends. BioMed Research International. 2021;2021(1):6634055. https://doi.org/10.1155/2021/6634055

3. Kligman S, Ren Z, Chung CH, Perillo MA, Chang YC, Koo H, Zheng Z, Li C. The impact of dental implant surface modifications on osseointegration and biofilm formation. Journal of clinical medicine. 2021 Apr 12;10(8):1641. https://doi.org/10.3390/jcm10081641

4. Hatamleh MM, Wu X, Alnazzawi A, Watson J, Watts D. Surface characteristics and biocompatibility of cranioplasty titanium implants following different surface treatments. Dental Materials. 2018 Apr 1;34(4):676-83. https://doi.org/10.1016/j.dental.2018.01.016

5. Mat-Baharin NH, Razali M, a Mohd-Said S, Syarif J, Muchtar A. Influence of alloying elements on cellular response and in-vitro corrosion behavior of titanium-molybdenum-chromium alloys for implant materials. Journal of Prosthodontic Research. 2020;64(4):490-7. https://doi.org/10.1016/j.jpor.2020.01.004

6. W. Nicholson J. Titanium alloys for dental implants: A review. Prosthesis. 2020 Jun 15;2(2):11. http://dx.doi.org/10.3390/prosthesis2020011

7. Elias CN, Fernandes DJ, de Souza FM, dos Santos Monteiro E, de Biasi RS. Mechanical and clinical properties of titanium and titanium-based alloys (Ti G2, Ti G4 cold worked nanostructured and Ti G5) for biomedical applications. Journal of Materials Research and Technology. 2019 Jan 1;8(1):1060-9. https://doi.org/10.1016/j.jmrt.2018.07.016

8. Jiman PA, Moldovan M, Sarosi C, Muntean A, Pop AS, Tarmure V, Popa C, Mohan AG. Surface characterization and cytotoxicity analysis of the titanium alloys for dentistry. Stud. Univ. Babes-Bolyai Chem. 2020 Mar 1;65:149-62. https://doi:10.24193/subbchem.2020.1.12

9. Knaus J, Schaffarczyk D, Cölfen H. On the future design of bio–inspired polyetheretherketone dental implants. Macromolecular bioscience. 2020 Jan;20(1):1900239. https://doi.org/10.1002/mabi.201900239

10. An F, Zhang B, Yan Y, Wang L. Effect of vanadium contents on microstructure and mechanical properties of Ti–6Al–xV components produced by wire+ Arc additive manufacturing. Materials Transactions. 2021 Aug 1;62(8):1071-8.. https://doi.org/10.2320/matertrans.MT-M2021031

11. Silva RC, Agrelli A, Andrade AN, Mendes-Marques CL, Arruda IR, Santos LR, Vasconcelos NF, Machado G. Titanium dental implants: an overview of applied nanobiotechnology to improve biocompatibility and prevent infections. Materials. 2022 Apr 27;15(9):3150. https://doi.org/10.3390/ma15093150

12. Sidhu SS, Singh H, Gepreel MA. A review on alloy design, biological response, and strengthening of β-titanium alloys as biomaterials. Materials Science and Engineering: C. 2021 Feb 1;121:111661. https://doi.org/10.1016/j.msec.2020.111661

13. Abd-elrhman Y, Gepreel MA, Abdel-Moniem A, Kobayashi S. Compatibility assessment of new V-free low-cost Ti–4.7 Mo–4.5 Fe alloy for some biomedical applications. Materials & Design. 2016 May 5;97:445-53. https://doi.org/10.1016/j.matdes.2016.02.110

14. Zhao X, Niinomi M, Nakai M, Ishimoto T, Nakano T. Development of high Zr-containing Ti-based alloys with low Young's modulus for use in removable implants. Materials Science and Engineering: C. 2011 Oct 10;31(7):1436-44. https://doi.org/10.1016/j.msec.2011.05.013

15. Ahmed DM, Omar SS. Cementing line configuration of bioactive engineered zirconia implants (in vivo histological study). Key Engineering Materials. 2018 Nov 30;786:236-47. http://dx.doi.org/10.4028/www.scientific.net/KEM.786.236

16. Smith MM. Orban oral histology and embryology: 11th edn. Pp. 478. 1991. SN Baskhar. London, Wolfe Publishing. Hardback,£ 29.95. https://www.amazon.com/Orbans-Oral-Histology-Embryology 11E/dp/8181470125

17. Ohshima S, Kobayashi H, Yamaguchi N, Nishioka K, Umeshita-Sasai M, Mima T, Nomura S, Kon S, Inobe M, Uede T, Saeki Y. Expression of osteopontin at sites of bone erosion in a murine experimental arthritis model of collagen-induced arthritis: Possible involvement of osteopontin in bone destruction in arthritis. Arthritis & Rheumatism: Official Journal of the American College of Rheumatology. 2002 Apr;46(4):1094-101. https://doi.org/10.1002/art.10143

18. Mostafa D, Kassem YM, Omar SS, Shalaby Y. Nano-topographical surface engineering for enhancing bioactivity of PEEK implants (in vitro—histomorphometric study). Clinical Oral Investigations. 2023 Nov;27(11):6789-99. https://doi.org/10.1007/s00784-023-05291-w

19. Geetha M, Mudali UK, Gogia AK, Asokamani R, Raj B. Influence of microstructure and alloying elements on corrosion behavior of Ti–13Nb–13Zr alloy. Corrosion Science. 2004 Apr 1;46(4):877-92. http://dx.doi.org/10.1016/S0010-938X(03)00186-0

20. W. Nicholson J. Titanium alloys for dental implants: A review. Prosthesis. 2020 Jun 15;2(2):11. https://doi.org/10.3390/prosthesis2020011

21. Elias CN, Fernandes DJ, de Souza FM, dos Santos Monteiro E, de Biasi RS. Mechanical and clinical properties of titanium and titanium-based alloys (Ti G2, Ti G4 cold worked nanostructured and Ti G5) for biomedical applications. Journal of Materials Research and Technology. 2019 Jan 1;8(1):1060-9. https://doi.org/10.1016/j.jmrt.2018.07.016

22. Liu X, Chen S, Tsoi JK, Matinlinna JP. Binary titanium alloys as dental implant materials—a review. Regenerative biomaterials. 2017 Oct;4(5):315-23. https://doi.org/10.1093/rb/rbx027

23. Pesode P, Barve S. A review—metastable β titanium alloy for biomedical applications. Journal of Engineering and Applied Science. 2023 Dec;70(1):25. https://doi.org/10.1186/s44147-023-00196-7

24. Kent D, Wang G, Dargusch M. Effects of phase stability and processing on the mechanical properties of Ti–Nb based β Ti alloys. Journal of the Mechanical Behavior of Biomedical Materials. 2013 Dec 1;28:15-25. https://doi.org/10.1016/j.jmbbm.2013.07.007

25. Niinomi M, Nakai M. Titanium-based biomaterials for preventing stress shielding between implant devices and bone. International journal of biomaterials. 2011;2011(1):836587. https://doi.org/10.1155/2011/836587

26. Ehtemam-Haghighi S, Liu Y, Cao G, Zhang LC. Phase transition, microstructural evolution and mechanical properties of Ti-Nb-Fe alloys induced by Fe addition. Materials & Design. 2016 May 5;97:279-86. https://doi.org/10.1016/j.matdes.2016.02.094

27. Chen LY, Cui YW, Zhang LC. Recent development in beta titanium alloys for biomedical applications. Metals. 2020 Aug 24;10(9):1139. https://doi.org/10.3390/met10091139

28. Elbanna AM, Salem KE, Mokhtar AM, Ramadan M, Elgamal M, Motaweh HA, Tourk HM, Gepreel MA, Allam NK. Ternary Ti–Mo–Fe nanotubes as efficient photoanodes for solar-assisted water splitting. The Journal of Physical Chemistry C. 2021 Jun 7;125(23):12504-17. https://doi.org/10.1021/acs.jpcc.1c01478

29. Mohan P, Osman TA, Amigo V, Mohamed A. Effect of Fe content, sintering temperature and powder processing on the microstructure, fracture and mechanical behaviours of Ti-Mo-Zr-Fe alloys. Journal of Alloys and Compounds. 2017 Dec 30;729:1215-25. https://doi.org/10.1016/j.jallcom.2017.09.255

30. Elias CN, Fernandes DJ, Resende CR, Roestel J. Mechanical properties, surface morphology and stability of a modified commercially pure high strength titanium alloy for dental implants. Dental Materials. 2015 Feb 1;31(2):e1-3. https://doi.org/10.1016/j.dental.2014.10.002

31. Datta S, Mahfouf M, Zhang Q, Chattopadhyay PP, Sultana N. Imprecise knowledge based design and development of titanium alloys for prosthetic applications. Journal of the mechanical behavior of biomedical materials. 2016 Jan 1;53:350-65. https://doi.org/10.1016/j.jmbbm.2015.08.039

32. Savio D, Bagno A. When the total hip replacement fails: A review on the stress-shielding effect. Processes. 2022 Mar 21;10(3):612. https://doi.org/10.3390/pr10030612

33. Cao S, Zhang ZM, Zhang JQ, Wang RX, Wang XY, Yang L, Chen DF, Qin GW, Zhang EL. Improvement in antibacterial ability and cell cytotoxicity of Ti–Cu alloy by anodic

oxidation. Rare Metals. 2022 Feb;41:594-609. https://doi.org/10.1007/s12598-021-01806-0

34. Qiu KJ, Liu Y, Zhou FY, Wang BL, Li L, Zheng YF, Liu YH. Microstructure, mechanical properties, castability and in vitro biocompatibility of Ti–Bi alloys developed for dental applications. Acta biomaterialia. 2015 Mar 15;15:254-65. https://doi.org/10.1016/j.actbio.2015.01.009

35. Castellano A, Gil LF, Bonfante EA, Tovar N, Neiva R, Janal MN, Coelho PG. Early healing evaluation of commercially pure titanium and Ti-6Al-4V presenting similar surface texture: An: In vivo: Study. Implant dentistry. 2017 Jun 1;26(3):338-44. https://doi.org/10.1097/id.0000000000000591

36. López-Valverde N, Aragoneses J, Rodríguez C, Aragoneses JM. Effect on osseointegration of dental implants treated with carboxyethylphosphonic acid and functionalized with BMP-2: preliminary study on a minipig model. Frontiers in Bioengineering and Biotechnology. 2023 Jul 27;11:1244667. http://dx.doi.org/10.3389/fbioe.2023.1244667